Journal of Power Sources 196 (2011) 2962–2970

Contents lists available at ScienceDirect

Journal of Power Sources

journal homepage: www.elsevier.com/locate/jpowsour

Review

Structure and performance of $LiFePO_4$ cathode materials: A review

Wei-Jun Zhang

Department of Mechanical Engineering, Virginia Commonwealth University, 401 West Main Street, Richmond, VA 23284, United States

ARTICLE INFO

Article history:
Received 1 October 2010
Received in revised form
12 November 2010
Accepted 22 November 2010
Available online 26 November 2010

Keywords:
Battery
$LiFePO_4$
Performance
Reaction mechanism
Carbon coating

ABSTRACT

$LiFePO_4$ has been considered a promising battery material in electric vehicles. However, there are still a number of technical challenges to overcome before its wide-spread applications. In this article, the structure and electrochemical performance of $LiFePO_4$ are reviewed in light of the major technical requirements for EV batteries. The rate capability, capacity density, cyclic life and low-temperature performance of various $LiFePO_4$ materials are described. The major factors affecting these properties are discussed, which include particle size, doping, carbon coating, conductive carbon loading and synthesis techniques. Important future research for science and engineering is suggested.

Contents

1. Introduction

$LiFePO_4$ has been selected as one of the primary battery materials for electric vehicle (EV) applications [1]. The main advantages of $LiFePO_4$ are its flat voltage profile, low material cost, abundant material supply and better environmental compatibility compared to other cathode materials [3–8]. The drawbacks of $LiFePO_4$ include its relatively low theoretical capacity, low density, poor electronic conductivity and low ionic diffusivity (Table 1). Moreover, the processing cost of $LiFePO_4$ is generally high because carbon coating or small particle size is required to obtain appropriate performance at high current rates.

Since its discovery in 1997 [9], great progress has been made in improving and understanding the structure, electrochemical performance and synthesis techniques of $LiFePO_4$ [10–161]. These

E-mail address: zweijun@vcu.edu

0378-7753/$ – see front matter © 2010 Elsevier B.V. All rights reserved.
doi:10.1016/j.jpowsour.2010.11.113

Table 1
Comparison of the properties of different cathodes in 18,650 cells [2].

Property	$LiAl_{0.05}Co_{0.15}Ni_{0.8}O_2$	$LiCoO_2$	$LiMn_2O_4$	$LiFePO_4$
Avg. voltage (V)	3.65	3.84	3.86	3.22
Theo. capacity (mAh g^{-1})	265	274	117	170
True density (g cm^{-3})	4.73	5.05	4.15	3.60
Specific energy (Wh kg^{-1})	219.8	193.3	154.3	162.9
Energy density (Wh L^{-1})	598.9	557.8	418.6	415.0
Materials' cost	1.628	1.824	1.159	1.219
Energy cost (Wh US$$^{-1}$)	6.08	5.05	5.97	6.31

Table 2
Summary of major requirements for HEV and PHEV batteries [1].

Characteristics	HEV	PHEV (10 miles)	PHEV (40 miles)
Pulse discharge power (kW 10 s^{-1})	25–40	38	46
Available energy (kWh)	0.3–0.5	3.4	11.6
Cycle life (charge sustaining, 50 Wh)	300,000	300,000	300,000
Cycle life (charge depleting)	N/A	5000	5000
Calendar life (years)	15	15 (35 °C)	15 (35 °C)
Maximum weight (kg)	40–60	60	120
Maximum volume (L)	32–45	40	80
Max. price ($) (100k units $year^{-1}$)	500–800	1700	3400
Operating temperature (°C)	−30 to +52	−0 to +52	−30 to +52

advances have been discussed in several elegant review articles [5–8]. The current work attempts to provide a brief overview of the major achievements and the remaining challenges related to EV applications. A realistic understanding of the promises and concerns of $LiFePO_4$ is important to the massive adoption of this material in the EV market.

According to the standard proposed by the US Department of Energy (Table 2), the major technical barriers that need to be addressed for the commercialization of high-energy batteries for PHEVs (plug-in hybrid electric vehicles) and high-power batteries for HEVs (hybrid electrical vehicles) are as follows [1]:

(1) *Performance*. Much higher energy densities are required to meet the volume/weight requirements; the cyclic stability and low-temperature performance must be improved.
(2) *Cost*. The current cost of the promising Li-ion batteries is approximately two to five times too high on a kWh basis due to the high cost of raw materials, cell packaging and manufacturing process.
(3) *Life*. A long calendar life of 15 years for both PHEV and HEV is anticipated to be difficult to achieve. Specifically, the impact of combined EV/HEV cycles and extended time in a high state of charge on the battery life is unknown.
(4) *Abuse tolerance*. Tolerance of abusive conditions must be addressed, such as short circuit, overcharge, over-discharge, and exposure to fire.

In this article, the current status of $LiFePO_4$ research is reviewed in light of these technical challenges. The paper starts with a brief summary on the Li insertion/extraction mechanism, discusses the electrochemical performance in terms of rate capability, capacity density, cyclic stability and low-temperature behavior, and then describes the major performance-controlling factors and future research needs.

2. Lithium insertion/extraction mechanism

2.1. Crystal structure

The triphylite $LiFePO_4$ belongs to the olivine family of lithium ortho-phosphates with an orthorhombic lattice structure in the space group *Pnma* [9–12]. The lattice parameters are $a = 10.33$ Å, $b = 6.01$ Å, $c = 4.69$ Å and $V = 291.2$ A^3. The structure consists of corner-shared FeO_6 octahedra and edge-shared LiO_6 octahedra running parallel to the *b*-axis, which are linked together by the PO_4 tetrahedra (Fig. 1). Upon delithiation, the Li ions are extracted to yield heterosite $FePO_4$ without changing the olivine framework [9,13]. However, the lattice constants are changed to $a = 9.81$ Å, $b = 5.79$ Å, $c = 4.78$ Å and $V = 271.5$ A^3 for $FePO_4$, which corresponds to a reduction in lattice volume by 6.77%, an increase in *c* by 1.9%, and a decrease in *a* and *b* by 5% and 3.7%, respectively.

Because the oxygen atoms are strongly bonded by both Fe and P atoms, the structure of $LiFePO_4$ is more stable at high temperatures than layered oxides such as $LiCoO_2$. $LiFePO_4$ is stable up to 400 °C, while $LiCoO_2$ starts to decompose at 250 °C [14–16]. The high lattice stability results in excellent cyclic performance and operation safety for $LiFePO_4$. However, the strong covalent oxygen bonds also lead to low ionic diffusivity (10^{-13} to 10^{-16} cm^2 s^{-1}) and poor electronic conductivity ($\sim 10^{-9}$ cm s^{-1}) [17]. The Li diffusion in $FePO_4$ is widely believed to be one dimensional along the *b*-axis [10,11,18].

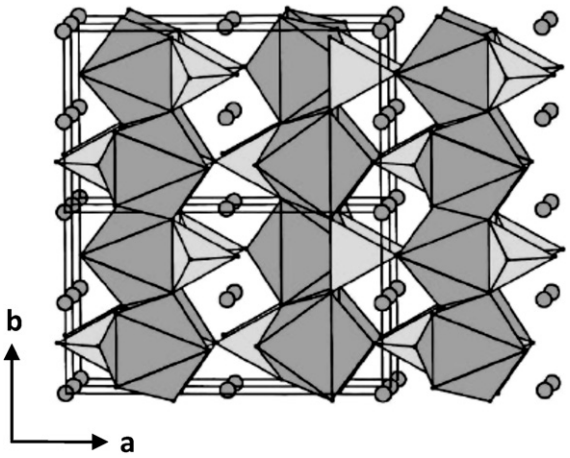

Fig. 1. The crystal structure of $LiFePO_4$ viewed along the *c*-axis [12]. The Fe atoms occupy octahedral (4c) sites (dark shading) and the P atoms occupy tetrahedral (4c) sites (light shading). The Li ions (small circles) occupy octahedral (4a) sites. Reproduced with permission from Elsevier.

2.2. Phase transformation

According to classical theory, the driving force for atom diffusion in a single phase is the concentration gradient. A higher concentration gradient results in fast atom diffusion. Unfortunately, such concentration gradients are rare in microsized Li_xFePO_4 particles due to the very limited solid-solution range for both $LiFePO_4$ and $FePO_4$ phases [19–21]. The solubility is believed to be less than 0.05 at room temperature for particles larger than 100 nm. At high temperatures, the miscibility gap between these two phases decreases [22,23]. The transformation from heterosite and triphylite phases to a disordered solid solution of Li_xFePO_4 takes place at approximately 200 °C. These two phases are entirely soluble at temperatures above 300 °C. Note that the phase diagram strongly depends on the particle size due to the surface energy effect [24,25]. The miscibility gap between $LiFePO_4$ and $FePO_4$ contracts when the particle sizes are reduced to less than 50 nm, and a completely solid solution is predicted for particles smaller than 15 nm at room temperature [26].

The phase transformation during Li insertion/extraction was initially proposed to follow the core–shell model or mosaic model [9,12]. According to these models, the shell of one phase covers the core of a second phase and the diffusion occurs through the shell with the movement of the interface. These models have been questioned based on the findings that the partially delithiated $LiFePO_4$ particles contain several $FePO_4$ domains and that the interfacial zones are not a solid solution but the superposition of two end phases [27–29]. Based on these observations, alternative models have been proposed including the "spinodal-decomposition model" [29] and the "domino-cascade model" [30]. Both models suggest that the Li insertion/extraction processes involve the cooperative motion of Li ions along the *b*-channels through the movement of phase boundaries (the nucleation front). Because the process is not diffusion-controlled in nature, no solid solution zones are required.

The mechanism proposed in these two models agrees well with the kinetic analysis of the process which indicates that the phase transformation is a phase-boundary controlled, one-dimensional process [31]. However, the main difference between these two models is the motion speed of the phase boundaries. The domino-cascade model claimed that the speed is extremely high so that no particles with the mixing phases are identified in the reaction process, therefore, the individual particles are either single triplylite or single heterosite [30]. The spinodal-decomposition model suggests that the movement of phase boundaries is relatively slow, and multiple domains and phase interfaces can be observed in the partially delithiated particles, as shown in Fig. 2. Note that the Li insertion/extraction processes in $LiFePO_4$ appear to depend on the particle size, synthesis method, surface coating, charging rate and testing procedures [33–36]. In nanosized particles, the phase transformation may deviate far from the equilibrium prediction for bulk materials because of the pronounced effect of surface and interface energies in small particles, which has been observed in Li_xTiO_2 and alloy anodes [37,38]. Therefore, more studies are warranted to understand the Li insertion/extraction mechanism in $LiFePO_4$ under real operation conditions using advanced in situ characterization tools.

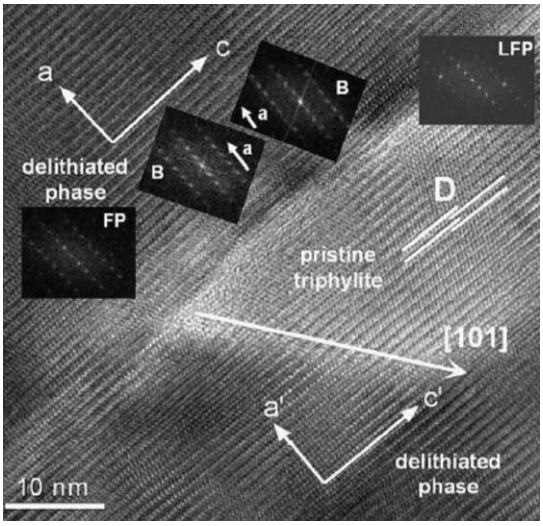

Fig. 2. HRTEM image of a partially delithiated $LiFePO_4$ particles showing a $LiFePO_4$ domain (LFP) in the *ac* plane surrounded by $FePO_4$ phase (FP) with narrow interface layers consisting of two crystal phases [29]. Reproduced with permission from Elsevier.

3. Electrochemical performance

3.1. Rate capability

The rate capability of $LiFePO_4$ has been extensively investigated due to the need for high pulse power in many applications. The rate capacity is affected by many factors, including particle size, doping, carbon coating, synthesis route, conductive carbon loading and the mixing procedure [39–44]. A comprehensive comparison of the rate capacity of various $LiFePO_4$ materials has been presented in a previous paper [45]. The analysis points out that the electric conductivity between the $LiFePO_4$ powders and the current collector plays a critical role in the high-rate performance of the battery cells. Carbon coating seems to improve the rate capacity of $LiFePO_4$ more effectively than particle size reduction and cation doping. Because the $LiFePO_4/FePO_4$ reaction is a non-diffusional, cooperative process as discussed above, the transport of Li ions and electrons through the particles is not expected to be the limiting process. Instead, the fast transport of electrons from the particle surface to the current collector is more critical, particularly at a high current rate, provided that the diffusion of Li-ions through the electrolyte to the graphite anode is not limited. Thus, carbon coating and conductive carbon loading are more likely to be important than particle size control and doping at high current rates.

As shown in Fig. 3, the materials prepared by polyol, direct-precipitation, sol–gel and ball-milling exhibit excellent high-rate capacities [45]. The microsized particles (DP-140, BM-C-300) exhibit excellent high-rate capacities, which are comparable to that of the best nanosized sample (PL-30). It is interesting to note the exceptional high-rate performance of the SS-50 material in Fig. 3, although the result was disputed by others [46,47]. This material is a non-stoichiometric $LiFePO_4$ prepared by a solid-state reaction (ball milling) and tested in a half cell using Li-metal as the anode. The superior performance of this material was attributed by the authors to its small particle size (50 nm) and the surface coating of pyrophosphates on the particles [48]. It will be interesting to evaluate this material in a full cell to examine its potential for practical application and to identify the impact of graphite anode on the rate performance of $LiFePO_4$/graphite full cell.

3.2. Capacity density

The specific energy ($Wh\,kg^{-1}$) and energy density ($Wh\,L^{-1}$) of battery cells are important parameters for EV and other applications. Increasing the specific energy significantly reduces the battery mass and cost, which are two of the major technical barriers to the wide-spread application of Li-ion batteries in EVs. The specific energy of battery cells is determined by many factors such as cell design, electrode structure, electrode potential and capacity

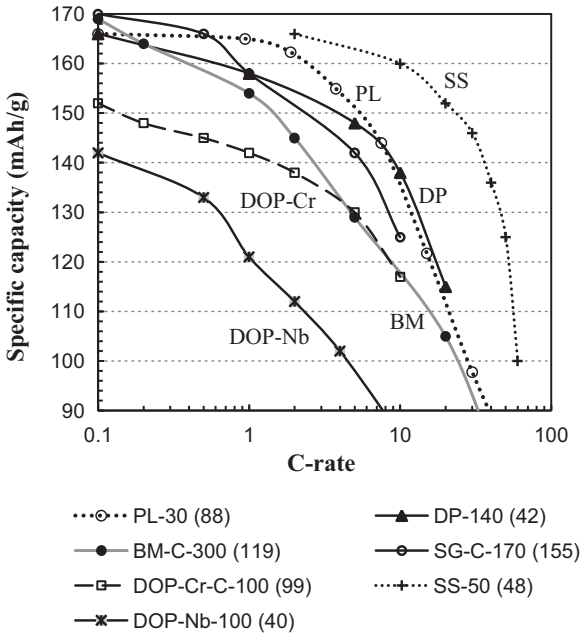

Fig. 3. Comparison of the rate capacities of $LiFePO_4$ materials prepared by different synthesis methods or with doping: PL (polyol), DP (direct-precipitation), SG (sol–gel), BM (ball-milling), SS (solid-state reaction) and DOP (doping) [45]. These samples represent the best materials from each category reported to date. The particle sizes and carbon coating (C) are indicated in the legend. Reproduced with permission from The Electrochemical Society.

[49,50]. Among these, the capacity density ($mAh\,L^{-1}$) of the cathode is one of the most critical factors because the active cathode materials account for approximately 40% by weight of the high-energy cells (Table 3).

The specific capacity ($mAh\,g^{-1}$) of $LiFePO_4$ has been widely investigated, and high specific capacities close to the theoretical value ($170\,mAh\,g^{-1}$) are obtained in a number of $LiFePO_4$ materials (Fig. 3). However, the energy density of battery cells is more correlated to the capacity density than the specific capacity. Due to carbon coating and particle size reduction, the tap densities of $LiFePO_4$ powders are generally low compared to those of other cathode materials [44,51,52]. For example, the nanosized $LiFePO_4$ materials have a tap density of 0.6–1.0 $g\,cm^{-3}$, while the commercial $LiCoO_2$ materials have a tap density of approximately 2.6 $g\,cm^{-3}$ [52,54,92]. A low tap density reduces energy density and increases the cell size and cost because more supporting materials such as electrolyte, separator and packaging materials, are needed as a result of less loaded active powders per volume or per area. The supporting materials account for a large portion of the mass and cost of battery cells, as shown in Tables 3 and 4. Therefore, high specific capacity does not necessarily lead to high energy density for $LiFePO_4$ if its tap density is low. In future studies, it is probably more meaningful to use capacity density, rather than specific capacity, to evaluate $LiFePO_4$ materials.

Table 3
Estimated material content of typical Li-ion cells [32].

Material/component	High-energy cell (100 Ah)		High-power cell (10 Ah)	
	Quantity (g)	wt.%	Quantity (g)	wt.%
Anode (dry)	785	23	56	17
Cathode (dry)	1610	47	93	29
Active material	1408	41	74	23
Electrolyte	618	18	44	13
Separators	60	1.8	16	5
Package (other)	358	10	115	35

Table 4
The estimated cost of major components in 18,650 cells with different cathodes [2].

Component/material	$LiAl_{0.05}Co_{0.15}Ni_{0.8}O_2$	$LiCoO_2$	$LiMn_2O_4$	$LiFePO_4$
Cathode	0.523	0.751	0.187	0.213
Anode	0.274	0.240	0.191	0.218
Electrolyte	0.267	0.296	0.296	0.276
Separator	0.174	0.156	0.130	0.140
Others	0.390	0.381	0.355	0.372
Total	1.628	1.824	1.159	1.219

The tap densities of microsized $LiFePO_4$ are in the range of 1.0–1.5 $g\,cm^{-3}$ [54–57]. New synthesis approaches have been explored recently to increase the tap density by controlling the morphology and size distribution of $LiFePO_4$ particles [51,54,58,59]. A high tap density of 1.8 $g\,cm^{-3}$ was achieved for a $LiFePO_4$/C composite containing 7 wt.% carbon prepared by a two-step drying process [54]. The composite shows a high specific capacity of 98 $mAh\,g^{-1}$ and a high capacity density of 167 $mAh\,cm^{-3}$ at 5 C rate. A $LiFePO_4$ material with a tap density of 1.3 $g\,cm^{-3}$ exhibits a high specific capacity of about 100 $mAh\,g^{-1}$ at 10 C rate [58]. When tested in a half-cell at a 30-min charge–discharge rate, excellent specific energy (440 $Wh\,kg^{-1}$) and power density (900 $W\,kg^{-1}$) were obtained although its specific capacity is not high compared to the best materials shown in Fig. 3.

3.3. Cyclic and calendar life

For batteries in both HEV and PHEV, the required cycle life at charge-sustaining mode (shallow-discharge) is 300,000 cycles and the expected calendar life is 15 years. In addition, a cycle life of 5000 cycles in the charge-depleting mode is required for PHEVs. These requirements are anticipated to be very challenging for any type of Li-ion batteries. For $LiFePO_4$ cathodes, long cyclic lives of 1500–2400 cycles have been achieved in laboratory tests [58–62]. However, the challenge is to develop adequate testing protocols that can effectively simulate and predict the battery performance in EV services [63]. To design appropriate testing procedures, it is necessary to understand the capacity-degradation mechanisms in both cycling (driving) and storage (parking) conditions.

The possible mechanisms of capacity degradation in $LiFePO_4$ cells include the following: (1) loss of Li inventory through a side reaction, (2) loss of active materials due to cracking and dissolution, (3) the rise of cell impedance due to the formation of SEI (surface–electrolyte-interface) layers, and (4) physical degradation of electrode structure [64–69]. Among these, the loss of Li-inventory due to SEI formation is considered to be the major cause [70,71]. Early studies have indicated that the SEI formation on graphite anode in $LiFePO_4$ cells is catalyzed and destabilized by the iron-deposits migrated from the $LiFePO_4$ cathode through the electrolyte [65,66]. Iron precipitates were observed on the surface of the graphite anode and on the separator [66,72,73]. The degree of capacity degradation seems to have a direct correlation with the iron content accumulated on the graphite anode [72,74]. It is believed that these irons are etched from the active $LiFePO_4$ particles by the acidic electrolyte solution. It was found that replacing the $LiPF_6$ salt with less-acidic LiBOB or $LiAlO_4$ salts in the electrolyte leads to much less iron dissolution and, therefore, much better capacity retention [65,75].

The dissolution rate of iron in an electrolyte also depends on the testing temperature, the cut-off voltage, the synthesis method, the impurity content and the particle size of $LiFePO_4$ [65,72–78]. Higher temperature, higher cut-off voltage (4.2 V), smaller particle size, and the presence of moisture or impurity phases such as $Fe_4(P_2O_7)_3$ lead to a higher rate of iron dissolution and faster capac-

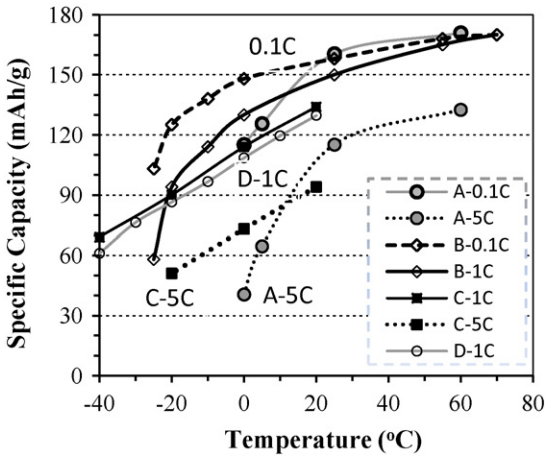

Fig. 4. The temperature dependence of specific capacities of $LiFePO_4$ materials tested in half-cells with different electrolytes: A: $LiClO_4$/EC-DMC [118], B: $LiPF_6$/EC-DMC [82], C: $LiPF_6$/EC-DMC-DEC-EMC [80], and D: $LiBF_4$–LiBOB/PC-EC-EMC [81].

ity fade. For example, the capacity retention of a $LiFePO_4$/graphite cell dropped from 100% to 57% after 100 cycles when the temperature was increased from 25 to 37 °C [65]. Replacing the graphite anode with Li-metal or $Li_4Ti_5O_{12}$ improved the capacity retention from about 30% to 90% at 55 °C after 100 cycles. The capacity retention can also be improved by coating the graphite anode or $LiFePO_4$ particles with polymer or oxide films to retard the iron dissolution and deposition [68,74,79]. The dissolution of iron has multiple detrimental effects: catalyzing the SEI formation on anode, reducing the inventory of active materials, and increasing the electric resistance. Mechanical cracking may also lead to the isolation of the active particles from the electrolyte or the conductive networks [67].

3.4. Temperature dependence

The poor performance of Li-ion batteries at low temperature is one of the major technical barriers for EV applications [1]. The operating temperature range for EV batteries is −40 °C to +50 °C. The specific capacities of $LiFePO_4$ have been observed to decrease rapidly at low temperature (especially below −20 °C), as shown in Fig. 4. The influence of temperature on the capacity is more pronounced at high charge rates. The loss of capacity at low temperature has been attributed to the limited electrode kinetics, low electrolyte conductivity, low Li diffusivity, and high charge-transfer resistance at the electrode/electrolyte interface [80–83]. As shown in Fig. 4, the low-temperature capacity can be improved by optimizing the Li-salts or the electrolyte solutions (samples C–D vs. A–B). The quaternary carbonate-based electrolyte (sample C) leads to better specific capacities at temperatures below −20 °C as compared to the binary electrolyte (samples A and B) [80]. The use of mixed $LiBF_4$–LiBOB salts in the electrolyte provides higher capacity over a wide temperature range (−50 to 80 °C) than $LiBF_4$ alone [81]. The influence of electrolyte formulation, carbon coating, particle size and surface structure of $LiFePO_4$ on the low-temperature performance deserves further evaluation. The influence of low temperature on the cycling stability of $LiFePO_4$ has also not been clearly understood yet. A study on a $LiFePO_4$/graphite cell with a polymer-gel electrolyte indicated that the cyclic capacity decreased more rapidly at 0 °C than at 25 °C [84].

At high temperatures, the specific capacities of $LiFePO_4$ are improved due to the increased lithium diffusion rate and electron transfer activity [15,85]. However, cycling or storing the $LiFePO_4$ cells at high temperature results in significant capacity fade [65,71,83]. The cause of capacity fade at elevated temperature has been attributed to the increased dissolution of Fe-ions from $LiFePO_4$ particles into the electrolyte, which are then deposited on the graphite anode surface. The deposited iron catalyzes the formation of SEI films, leading to an increase of interfacial impedance of graphite electrodes [65]. The high temperature stability was improved with a LiBOB electrolyte or $Li_4Ti_5O_{12}$ anode [34,65].

4. Factors affecting performance and energy cost

The electrochemical performance and energy cost of $LiFePO_4$ batteries are affected by many factors such as the electrolyte, separator and electrode materials. In this section, the major contributors related to the $LiFePO_4$ cathode are discussed.

4.1. Particle size

Particle size reduction has been employed in a number of studies as an effective method to improve the high-rate capacity and cycling stability of $LiFePO_4$ materials [42,48,86–88]. The capacities of $LiFePO_4$ at high current rates are believed by many to originate from its low ionic conductivity [89]. Logically, the high-rate performance can be improved by reducing particle size because the transport distance for electrons and Li-ions is thus reduced. In fact, the best high-rate performance for $LiFePO_4$ was achieved in the samples with very small particle size (30–50 nm), e.g., PL-30 and SS-50 in Fig. 3.

However, a recent analysis [45] of over 40 different $LiFePO_4$ materials reported in the literature indicates that the specific capacity of $LiFePO_4$ has no clear dependence on the particle size in the range 50–400 nm at 0.1 C and 1 C rates as shown in Fig. 5, which is contrary to a previous analysis [89] which concluded that the capacity of $LiFePO_4$ depends solely on the mean particle size. Even at 10 C rate, the specific capacities of microsized $LiFePO_4$ samples (200–300 nm) with carbon coating are comparable to those of many nanosized samples. The lack of direct correlation between the specific capacity and particle size may be related to the cooperative Li-movement process during Li insertion/extraction as discussed above. Because the transport of Li-ions in these particles is not diffusion-controlled, particle size reduction may not lead to as much improvement as expected in the size range of interest.

As mentioned in Section 2, the phase transformation in $LiFePO_4$ particles smaller than 50 nm is likely to be different from that in microsized particles. Thus, it is possible that these particles may exhibit superior capacity at high current rates. However, the capacity gain in nanosized $LiFePO_4$ materials may be not enough to offset their many adverse effects in real applications, although further research on these tiny particles is of scientific significance. The tap densities of nanoparticles are generally low, while their manufacturing costs are often high compared to microsized particles, leading to low energy density and high energy cost of the cells. Smaller particles also require more supporting materials such as conductive carbon, binder and current collector in a battery cell [49]. Due to their high surface areas and less-coordinated surface atoms, nanoparticles are more prone to surface reaction and particle dissolution in electrolyte, which may severely reduce the cyclic and calendar life of battery cells [90]. Processing and handling of nanoparticles are difficult and require extra precaution due to the health and environmental concerns. Therefore, the optimum particle size for high-power applications seems to be in the range of 200–400 nm, as estimated from the data shown in Fig. 5. The ideal particle size may be even larger for high-energy applications such as in PHEVs, where the energy density, battery mass and energy cost are more important than the high-rate capacity.

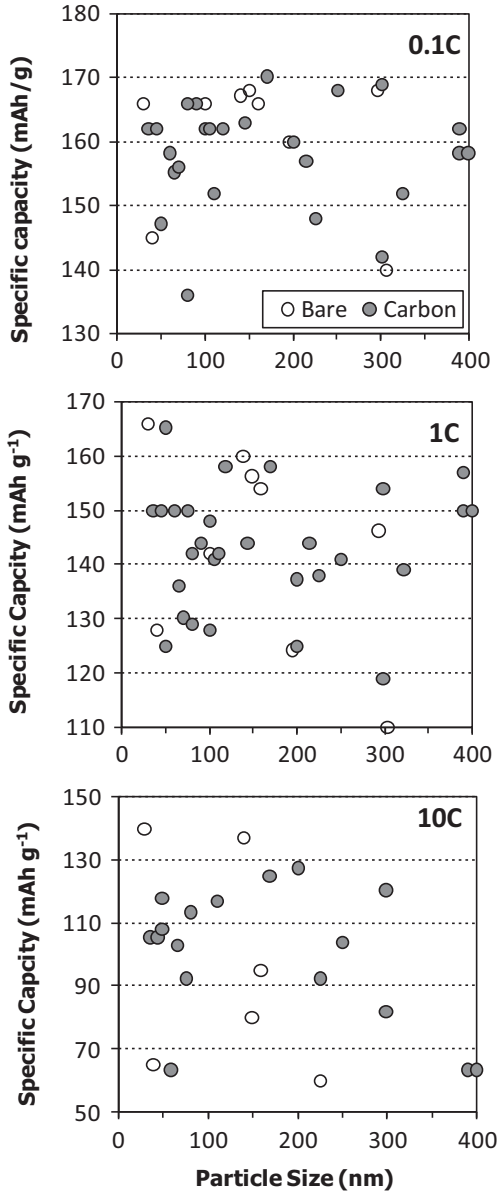

Fig. 5. The dependence of specific capacity at 0.1 C, 1 C and 10 C rates on the particle size of $LiFePO_4$ with or without carbon coating [45]. Reproduced with permission from The Electrochemical Society.

4.2. Doping

The positive effect of doping on the rate capacity and cyclic stability of $LiFePO_4$ has been reported in a group of studies [40,91–102]. The studied dopants include supervalent cations such as Nb^{5+} [40], Zr^{4+} [91], Ti^{4+} [91], Mo^{6+} [95], Mg^{2+} [93,100], Cr^{3+} [92,99], V^{5+} [94], Co^{2+} [96], Cu^{2+} [97], and anions of Cl^{-1} [102] and F^{-1} [101]. The promoting effect was attributed to the improved intrinsic electronic conductivity and the increased Li-ion diffusion coefficient in doped $LiFePO_4$ particles [98–103]. The electronic conductivity of $LiFePO_4$ powders was reported to increase by two to eight orders of magnitude as a result of doping-induced charge compensation [40,98,100].

However, the improvement in electronic conductivity was questioned by others to arise from the formation of conductive surface films (e.g., carbon, Fe_2P or $Fe_{75}P_{15}C_{10}$), as confirmed by TEM observations [104–106]. Modeling studies also suggested that supervalent doping on either Li or Fe sites is energetically unfavorable and does not result in a large increase of electronic conductivity [11,107]. Neutron and XRD studies revealed that the doped Zr, Nb and Cr atoms in $LiFePO_4$ are located primarily on the Li sites and, thus, may hinder the Li diffusion by blocking the Li-diffusion channels [108]. In terms of electrochemical property, the doped $LiFePO_4$ materials do not show significant advantages over the undoped samples [45]. For example, the specific capacities of the doped sample without carbon coating (DOP-Nb-100) are much lower than those of other materials despite of its small particle size (100 nm) (Fig. 3). Therefore, doping does not appear to be as effective as carbon coating for engineering applications, especially when taking into account the impact of doping (e.g., Nb and Mo) on the cost of raw materials. For the anion-doped $LiFePO_4$ (Cl^{-1} and F^{-1}) [101,102], the impact of doping on their structural stability and abuse tolerance at high temperature needs to be examined.

4.3. Carbon coating

Carbon coating is one of the most important techniques used to improve the specific capacity, rate performance and cycling life of $LiFePO_4$ [109–115]. The main role of carbon coating is to enhance the surface electronic conductivity of $LiFePO_4$ particles so that the active materials can be fully utilized at high current rates. Carbon coating also reduces the particle size of $LiFePO_4$ by inhibiting particle growth during sintering [116–118]. In addition, carbon can act as a reducing agent to suppress the oxidation of Fe^{2+} to Fe^{3+} during sintering and thus simplify the atmosphere requirement in synthesis [119,120]. With carbon coating, the microsized particles of ~300 nm exhibit good rate capability that is comparable to those of the nanosized particles, as shown in Fig. 5. The beneficial effect of carbon coating has been observed to depend on the structure, uniformity, thickness, loading and precursor of the coating [110–112,121–123]. The disadvantages of carbon coating include high processing cost and reduced tap density, which may lead to high energy cost and low energy density of the battery cells [44,52]. Therefore, it is important to optimize the carbon coating on $LiFePO_4$ to meet the performance and cost targets for EV applications.

Carbon coating on $LiFePO_4$ can be prepared with pre-existing carbon powders or by in situ carbonization of organic precursors [124–129]. It is now commonly believed that the carbon coatings formed in situ perform much better than the pre-existing carbons [125]. The structure and electronic conductivity of carbon coating produced from organic precursors are strongly influenced by the pyrolysis temperature and the precursor type [110,112]. Carbon coatings prepared at high temperature (>700 °C) have much higher electronic conductivity than those prepared at low temperature (<600 °C) as result of the increased amount of graphite carbon in the coating [110,119]. Graphite carbons (sp^2-coordinated) are more conductive than disordered carbons (sp^3-coordinated). The amount of graphite carbon in the coating can be determined from the band-intensity ratio of graphite (I_G) and disordered carbon (I_D) on the Raman spectra [110,121]. High electronic conductivity and better performance are achieved by using organic precursors having carbon-ring structures, such as polystyrene and sugar [44,111,121,119,130]. With high-quality carbon coatings, the amount of conductive carbons used in cathode preparation can be reduced [49,131]. The ideal carbon coating needs to be dense, uniform, graphite-like, 2–3 nm thick and 1–3 wt.% [49,123].

Coating the $LiFePO_4$ particles with other conductive films, such as polypyrrole or Fe_2P, also improves their electrochemical performance [74,111,117,132].

4.4. Conductive carbon

Conductive carbon powders are added in the cathode to improve the electronic contact between the active powders and the elec-

tronic conductor. The loading of conductive carbon and the mixing procedure significantly affect the electrochemical performance of the prepared cells [39,42–45]. Higher conductive carbon loading generally improves the rate capacity but reduces the energy density of the cells. In addition, a uniform distribution of the conductive carbon particles in the cathode through extensive or wet mixing is also important [39,42,43,49]. The influence of particle size, loading and mixing procedure of conductive carbons on the performance of battery cells needs further attentions.

4.5. Synthesis methods

The $LiFePO_4$ powders have been prepared by a variety of synthesis techniques, including ball milling [133–137], solid-state reaction [40,138], microwave [139–141], carbothermal reduction [142–145], hydrothermal reaction [146–150], co-precipitation [14,151], sol–gel [152–155], spray-pyrolysis [41,156,157], and rheological method [158–160]. For large-scale industrial applications, low processing cost and easy manufacturing are the primary requirements for any synthesis methods. Therefore, the current discussion concentrates on two processes that have been used for commercial production: mechanochemical activation (MA) and carbothermal reduction (CR), although excellent performance has been achieved in materials prepared by other methods [7].

In the MA process, the precursors, such as Li_2CO_3, FeC_2O_4, $NH_4H_2PO_4$ and sucrose, are thoroughly crushed and mixed in a high energy ball mill; as a result, the sintering temperature and time necessary to obtain a fully crystallized material is reduced and small particle size is maintained [22,119,136]. The milling time is normally 4–24 h, and the optimum sintering conditions are reported to be 600–700 °C for 4–24 h, varied in different studies [119,135,137,161]. At high sintering temperatures, the formation of impurity phases, such as Fe_2P and Fe_3P, were observed. The presence of Fe_2P impurities decreases the capacity density and the cyclic stability of $LiFePO_4$. The disadvantages of this process are its long processing cycle and high energy consumption, which inevitably increase the manufacturing cost. In addition, the particle size distribution of MA powders is relatively broad. To reduce the processing cost, additional studies are needed to understand the structure and surface change during sintering and to shorten the processing cycle while maintaining good electrochemical properties. The sintering time can be reduced by increasing the sintering temperature when the carbon coating is present [162]. Sintering at high temperatures improves the electronic conductivity of carbon coating, while a short sintering time and fast cooling inhibit particle growth. For massive industrial production, a continuous manufacturing process is highly desired, especially when advanced heating techniques such as infrared or laser heating are employed.

In the CR process, a low-cost Fe^{3+}-precursor such as Fe_2O_3 or $FePO_4$ is used as Fe source instead of the expensive Fe^{2+} precursors, e.g., FeC_2O_4 and $Fe(OOCH_3)_2$ [142,145,158,160]. The Fe^{3+} is reduced by the fresh formed carbon from the pyrolysis of precursors during sintering. Thus, the cost of CR-$LiFePO_4$/carbon is expected to be low while their tap density is relatively high. Similar to the MA method, the CR process needs to be further optimized to reduce the processing time and energy consumption while maintaining the performance by controlling the particle size and impurity content.

5. Future research needs

It is of scientific and engineering importance to understand the Li insertion/extraction mechanism under real operation conditions and at low temperatures. Further investigation on the phase transformation in nanosized $LiFePO_4$ particles (<40 nm) is also merited. To clarify the effect of doping on the electronic and ionic conductivity of $LiFePO_4$, well-designed experiments are needed to exclude the contribution of other factors, such as surface coating or particle size. For engineering applications, more efforts are warranted to prepare $LiFePO_4$ materials with a combination of good performance, high tap density and low processing cost. Modeling and experimental works on the electrode structure design are required to increase the energy density of battery cells. In addition, the abuse tolerance, low-temperature performance and the long-term stability of $LiFePO_4$ under the combined EV/HEV cycles warrant further study.

6. Conclusions

The phase transformation and electrochemical performance of various $LiFePO_4$ materials are discussed in light of the technical requirements for EV batteries. The Li insertion/extraction processes in $LiFePO_4$ appear to take place through the cooperative motion of electrons and Li-ions along the phase boundaries. As a result, the rate capability of $LiFePO_4$ is mainly affected by the transport of electrons from the particle surface to the current collector. Carbon coating and conductive carbon loading are more critical than doping and particle size control when the particles are smaller than 400 nm.

The cyclic life of $LiFePO_4$ has been significantly improved to over 2000 cycles. The migration of iron from the cathode onto the surface of graphite anode through electrolyte has been reported to be mainly responsible for the capacity degradation because the deposited iron catalyzes the SEI formation on the anode. Thus, the cycling life of $LiFePO_4$ cathode under the combined calendar/cyclic cycles needs to be carefully evaluated for EV applications. The low-temperature performance of $LiFePO_4$ can probably be improved by developing novel electrolyte formulations. To meet the stringent technical requirements for EVs, more effort is required to increase the energy density and reduce the energy cost of $LiFePO_4$ batteries.

Acknowledgements

The author would like to thank Prof. Gary Tepper and Dr. Russell Jamison for a visiting professorship at Virginia Commonwealth University.

References

[1] D. Howell, DOE Energy Storage Research and Development, Annual Progress Report, 2008.
[2] W.F. Howard, R.M. Spontnitz, J. Power Sources 165 (2007) 887.
[3] A. Ritchie, W. Howard, J. Power Sources 162 (2006) 809.
[4] J.M. Tarascon, M. Armand, Nature 414 (2001) 359.
[5] M.S. Whittingham, MRS Bull. 33 (2008) 411.
[6] T. Ohzuhu, R.J. Brodd, J. Power Sources 174 (2007) 449.
[7] D. Jugovic, D. Uskokovic, J. Power Sources 190 (2009) 538.
[8] B. Scrosati, J. Garche, J. Power Sources 195 (2010) 2419.
[9] A.K. Pahdi, K.S. Nanjundaswamy, J.B. Goodenough, J. Electrochem. Soc. 144 (1997) 1188.
[10] J. Li, W. Yao, S. Martin, D. Vaknin, Solid State Ionics 179 (2008) 2016.
[11] C.A. Fisher, V.M. Hart Prieto, M.S. Islam, Chem. Mater. 20 (2008) 5907.
[12] A.S. Andersson, J.O. Thomas, J. Power Sources 97 (2001) 498.
[13] A.S. Andersson, B. Kalska, L. Haggstrom, J.O. Thomas, Solid State Ionics 130 (2000) 41.
[14] G. Atnold, J. Garche, R. Hemmer, S. Strobele, C. Vogler, M. Wohlfahrt-Mehrens, J. Power Sources 119 (2003) 247.
[15] M. Takahashi, S. Tobishima, K. Takei, Y. Sakurai, Solid State Ionics 148 (2002) 283.
[16] J.R. Dahn, E.W. Fuller, M. Obrovac, U. von Sacken, Solid State Ionics 69 (1994) 265.
[17] X.C. Tang, L.X. Li, Q.L. Lai, X.W. Song, L.H. Jiang, Electrochem. Acta 54 (2009) 2329.
[18] D. Morgan, A. Van der Ven, G. Ceder, Electrochem. Solid-State Lett. 7 (2004) A30.
[19] A. Yamada, H. Koizumi, S.I. Nishimura, N. Sonoyama, R.J. Kanno, M. Yonemura, T. Nakamura, Y. Kobayashi, Nat. Mater. 5 (2006) 357.
[20] V. Srinivasan, J. Newman, J. Electrochem. Soc. 151 (2004) A1517.

[21] A. Yamada, H. Koizumi, N. Sonoyama, R. Kanno, Electrochem. Solid State Lett. 8 (2005) A409.
[22] J.L. Dodd, R. Yamazi, B. Fultz, Electrochem. Solid State Lett. 9 (2006) A151.
[23] C. Delacourt, P. Poizot, J.M. Tarascon, C. Masquelier, Nat. Mater. 4 (2005) 254.
[24] N. Meethong, H.S. Huang, S.A. Speakman, W.C. Carter, Y.M. Chiang, Adv. Funct. Mater. 17 (2007) 1115.
[25] M. Wagemaker, F.M. Mulder, A. Van der Ven, Adv. Mater. 21 (2009) 2703.
[26] N. Meethong, H.S. Huang, W.C. Carter, Y.M. Chiang, Electrochem. Solid State Lett. 10 (2007) A134.
[27] G. Chen, X. Song, T.J. Richardson, Electrochem. Solid State Lett. 9 (2006) A295.
[28] L. Laffont, C. Delacourt, P. Gibot, M.Y. Wu, P. Kooyman, C. Masquelier, J.M. Tarascon, Chem. Mater. 18 (2006) 5520.
[29] C.V. Ramana, A. Mauger, F. Gendron, C.M. Julien, K. Zaghib, J. Power Sources 187 (2009) 555.
[30] C. Delmas, M. Maccario, L. Croguennec, F. Le Cras, F. Weill, Nat. Mater. 7 (2008) 665.
[31] J.L. Allen, T.R. Jow, J. Wolfenstine, Chem. Mater. 19 (2007) 2108.
[32] L. Gaines, R. Cuenca, Cost of lithium-ion batteries for vehicles, Report #ANL/ESD-42, Argonne National Laboratory, May 2000.
[33] P. Gibot, M. Casas-Cabanas, L. Laffont, S. Levasseur, P. Carlach, S. Hamelet, J.M. Tarascon, C. Masquelier, Nat. Mater. 7 (2008) 741.
[34] F. Mestre-Aizpurua, S. Hamelet, C. Masquelier, M.R. Palacin, J. Power Sources 195 (2010) 6897.
[35] H.H. Chang, C.C. Chang, H.C. Wu, M.H. Yang, H.S. Sheu, N.L. Wu, Electrochem. Commun. 10 (2008) 335.
[36] H.C. Shin, K.Y. Chuang, W.S. Min, D.J. Byun, H. Jang, B.W. Cho, Electrochem. Commun. 10 (2008) 536.
[37] W.J. Zhang, J. Power Sources 196 (2011) 877.
[38] M. Wagemaker, W.J.H. Borghols, F.M. Mulder, J. Am. Chem. Soc. 129 (2007) 4323.
[39] R. Dominko, M. Gaberscek, J. Drofenik, M. Bele, S. Pejovnik, J. Jamnik, J. Power Sources 119–121 (2003) 770.
[40] S.Y. Chung, J.T. Bloking, Y.T. Chiang, Nat. Mater. 1 (2002) 123.
[41] F. Yu, J. Zhang, Y. Yang, G. Song, J. Power Sources 189 (2009) 794.
[42] C. Delacourt, P. Poizot, S. Levasseur, C. Masquelier, Electrochem. Solid-State Lett. 9 (2006) A352.
[43] D. Zane, M. Carewska, S. Scaccia, F. Cardellini, P.P. Prosini, Electrochem. Acta 49 (2004) 4259.
[44] Z. Chen, J.R. Dahn, J. Electrochem. Soc. 149 (2002) A1184.
[45] W.J. Zhang, J. Electrochem. Soc. 157 (2010) A1040.
[46] G. Ceder, B. Kang, J. Power Sources 194 (2009) 1024.
[47] K. Zaghib, J.B. Goodenough, A. Mauger, C. Julien, J. Power Sources 194 (2009) 1021.
[48] B.K. Kang, G. Ceder, Nature 458 (2009) 190.
[49] A. Awarke, S. Lauer, S. Pischinger, M. Wittler, J. Power Sources 196 (2011) 405.
[50] W. Lu, A. Jansen, D. Dees, P. Nelson, N.R. Veselka, G. Henriksen, J. Power Sources 196 (2011) 1537.
[51] S.W. Oh, S.T. Myung, S.M. Oh, C.S. Yoon, K. Amine, Y.K. Sun, Electrochem. Acta 55 (2010) 1193.
[52] S.T. Yang, N.H. Zhao, H.Y. Dong, J.X. Yang, H.Y. Yue, Electrochem. Acta 51 (2005) 166.
[53] P. He, H. Wang, L. Qi, T. Osaka, J. Power Sources 158 (2006) 529.
[54] Z.R. Chang, H.J. Lv, H.W. Tang, H.J. Li, X.Z. Yuan, H. Wang, Electrochem. Acta 54 (2009) 4595.
[55] J.M. Chen, C.H. Hsu, Y.R. Lin, M.H. Hsiao, G.T. Fey, J. Power Sources 184 (2008) 498.
[56] J.F. Ni, H.H. Zhou, J.T. Chen, X.X. Zhang, Mater. Lett. 61 (2007) 1260.
[57] L.Q. Sun, R.H. Cui, A.F. Jalbout, M.J. Li, X.M. Pan, R.S. Wang, H.M. Xie, J. Power Sources 189 (2009) 522.
[58] J. Liu, J. Wang, X. Yan, X. Zhang, G. Yang, A.F. Jalbout, R. Wang, Electrochem. Acta 54 (2009) 5656.
[59] M.E. Zhong, Z.T. Zhou, Mater. Chem. Phys. 119 (2010) 428.
[60] Y.J. Gu, C.S. Zeng, H.K. Wu, H.Z. Cui, X.W. Huang, X.B. Liu, C.L. Wang, Z.N. Yang, H. Liu, Mater. Lett. 61 (2007) 4700.
[61] S.B. Peterson, J. Apt, J.F. Whiteacre, J. Power Sources 195 (2010) 2385.
[62] X. Yan, G. Yang, J. Liu, Y. Ge, H. Xie, X. Pan, R. Wang, Electrochem. Acta 54 (2009) 5770.
[63] M. Dubarry, V. Svoboda, R. Hwu, B.Y. Liaw, J. Power Sources 174 (2007) 366.
[64] J. Shim, K.A. Striebel, J. Power Sources 119 (2003) 955.
[65] K. Amine, J. Liu, I. Belharouak, Electrochem. Commun. 7 (2005) 669.
[66] K. Striebel, J. Shim, A. Sierra, H. Yang, X. Song, R. Kostecki, K. McCarthy, J. Power Sources 146 (2005) 33.
[67] D. Wang, X. Wu, Z. Wang, L. Chen, J. Power Sources 140 (2005) 125.
[68] H.H. Chang, H.C. Wu, N.L. Wu, Electrochem. Commun. 10 (2008) 1823.
[69] Q. Zhang, R.E. White, J. Power Sources 173 (2007) 990.
[70] M. Dubarry, B.Y. Liaw, J. Power Sources 194 (2009) 541.
[71] M. Dubarry, B.Y. Liaw, M.S. Chen, S.S. Chyan, K.C. Han, W.T. Sie, S.H. Wu, J. Power sources (2011), doi:10.1016/j.jpowsour.2010.07.029 (article online).
[72] H.F. Jin, Z. Liu, Y.M. Teng, J.K. Gao, Y. Zhao, J. Power Sources 189 (2009) 445.
[73] K. Zaghib, N. Ravet, M. Gauthier, F. Gendron, A. Mauger, J.B. Goodenough, C.M. Julien, J. Power Sources 163 (2006) 560.
[74] Y. Yang, X.Z. Liao, Z.F. Ma, B.F. Wang, L. He, Y.S. He, Electrochem. Commun. 11 (2009) 1277.
[75] M. Koltypin, D. Aurbach, L. Nazar, B. Ellis, J. Power Sources 174 (2007) 1241.
[76] D. Aurbach, B. Markovsky, G. Salitra, E. Markevich, Y. Talyossef, M. Koltypin, L. Nazar, B. Ellis, D. Kovacheva, J. Power Sources 165 (2007) 491.
[77] X. Zhi, G. Liang, L. Wang, X. Ou, J. Zhang, J. Cui, J. Power Sources 189 (2009) 779.
[78] N. Iltchev, Y. Chen, S. Okada, J. Yamaki, J. Power Sources 119 (2003) 749.
[79] G.M. Song, Y. Wu, G. Liu, Q. Xu, J. Alloys Compd. 487 (2009) 214.
[80] X.Z. Liao, Z.F. Ma, Q. Gong, Y.S. He, L. Pei, L.J. Zeng, Electrochem. Commun. 10 (2008) 691.
[81] S.S. Zhang, K. Xu, T.R. Jow, J. Power Sources 159 (2006) 702.
[82] S. Franger, C. Benoit, C. Bourbon, F. Le Cras, J. Phys. Chem. Solids 67 (2006) 1338.
[83] H.S. Kim, B.W. Cho, W.I. Cho, J. Power Sources 132 (2004) 235.
[84] K. Zaghib, K. Striebel, A. Guerfi, J. Shim, M. Armand, M. Gauthier, Electrochem. Acta 50 (2004) 263.
[85] S.H. Wu, K.M. Hsiao, W.R. Liu, J. Power Sources 146 (2005) 550.
[86] C.R. Sides, F. Croce, V.Y. Young, C.R. Martin, B. Scrosati, Electrochem. Solid State Lett. 8 (2005) A484.
[87] G.T. Fey, Y.G. Chen, H.M. Kao, J. Power Sources 189 (2009) 169.
[88] D.H. Kim, J. Kim, Electrochem. Solid-State Lett. 9 (2006) A439.
[89] M. Gaberscek, R. Dominko, J. Jamnik, Electrochem. Commun. 9 (2007) 2778.
[90] J. Jamnik, J. Maier, Phys. Chem. Chem. Phys. 5 (2003) 5215.
[91] G.X. Wang, S. Needham, J. Yao, J.Z. Wang, R.S. Liu, H.K. Liu, J. Power Sources 159 (2006) 282.
[92] J. Ying, M. Lei, C. Jiang, C. Wan, X. He, J. Li, L. Wang, J. Ren, J. Power Sources 158 (2006) 543.
[93] M.R. Roberts, G. Vintins, J.R. Owen, J. Power Sources 179 (2008) 754.
[94] Y. Wen, L. Zeng, Z. Tong, L. Nong, W. Wei, J. Alloys. Compd. 416 (2006) 206.
[95] M. Zhang, L.F. Jiao, H.T. Yuan, Y.M. Wang, J. Guo, M. Zhao, W. Wang, X.D. Zhou, Solid State Ionics 177 (2006) 3309.
[96] D. Wang, H. Li, S. Shi, X. Huang, L. Chen, Electrochem. Acta 50 (2005) 2955.
[97] R. Yang, X. Song, M. Zhao, F. Wang, J. Alloys Compd. 468 (2009) 365.
[98] G.X. Wang, S.L. Bewlay, K. Konstantinov, H.K. Liu, S.X. Dou, J.H. Ahn, Electrochem. Acta 50 (2004) 443.
[99] H.C. Shin, S.B.H. Park, J.K.Y. Chuang, W. Cho, C.S. Kim, B.W. Cho, Electrochim. Acta 53 (2008) 7946.
[100] T.H. Teng, M.R. Yang, S.H. Wu, Y.P. Chiang, Solid State Commun. 142 (2007) 389.
[101] X.Z. Liao, Y.S. He, Z.F. Ma, X.M. Zhang, L. Wang, J. Power Sources 174 (2007) 720.
[102] C.S. Sun, Y. Zhang, X.J. Zhang, Z. Zhou, J. Power Sources 195 (2010) 3680.
[103] C.S. Sun, Z. Zhou, Z.G. Xu, D.G. Wang, J.P. Wei, X.K. Bian, J. Yan, J. Power Sources 193 (2009) 841.
[104] N. Ravet, A. Abouimrane, M. Armand, Nat. Mater. 2 (2003) 702.
[105] C. Delacourt, C. Wurm, L. Laffont, J.B. Leriche, C. Masquelier, Solid State Ionics 177 (2006) 333.
[106] P.S. Herle, B. Ellis, N. Coombs, L.F. Nazar, Nat. Mater. 3 (2004) 147.
[107] J. Xu, G. Chen, Physica B 405 (2010) 803.
[108] M. Wagemaker, B.L. Ellis, D. Lutzenkirchen-Hecht, F.M. Mulder, L.F. Nazar, Chem. Mater. 20 (2008) 6313.
[109] H. Huang, S.C. Yin, L.F. Nazar, Electrochem. Solid State Lett. 4 (2001) A170.
[110] M.M. Doeff, Y. Hu, F. McLarnon, R. Kostecki, Electrochem. Solid State Lett. 6 (2003) A207.
[111] Y. Kadoma, J.M. Kim, K. Abiko, K. Ohtsuki, K. Ui, N. Kumagai, Electrochem. Acta 55 (2010) 1034.
[112] M.M. Doeff, J.D. Wilcox, R. Kostecki, G. Lau, J. Power Sources 163 (2006) 180.
[113] S.T. Myung, S. Komaba, N. Hirosaki, H. Yashiro, N. Kumagai, Electrochem. Acta 49 (2004) 4213.
[114] J.K. Kim, G. Cheruvally, J.H. Ahn, G.C. Hwang, J.B. Choi, J. Phys. Chem. Solids 69 (2008) 2371.
[115] Y. Ding, Y. Jiang, F. Xu, J. Yin, H. Ren, Q. Zhuo, Z. Long, P. Zhang, Electrochem. Commun. 12 (2010) 10.
[116] M.A.E. Sanchez, G.E.S. Brito, M.C.A. Fantini, G.F. Goya, J.R. Matos, Solid State Ionics 177 (2006) 497.
[117] Y. Lin, M.X. Gao, D. Zhu, Y.F. Liu, H.G. Pan, J. Power Sources 184 (2008) 444.
[118] S.A. Needham, A. Calka, G.X. Wang, A. Mosbah, H.K. Liu, Electrochem. Commun. 8 (2006) 434.
[119] K. Wang, R. Cai, T. Yuan, X. Yu, R. Ran, Z. Shao, Electrochem. Acta 54 (2009) 2861.
[120] G.R. Hu, X.G. Gao, Z.D. Penh, K. Du, Y.J. Liu, Chin. Chem. Lett. 18 (2007) 337.
[121] Y.H. Nien, J.R. Carey, J.S. Chen, J. Power Sources 193 (2009) 822.
[122] Y.D. Cho, G.T.K. Fey, H.M. Kao, J. Power Sources 189 (2009) 256.
[123] R. Dominko, M. Bele, M. Gaberscek, M. Remskar, D. Hanzel, S. Pejovnik, J. Jamnik, J. Electrochem. Soc. 152 (2005) A607.
[124] S.S. Zhang, J.L. Allen, K. Xu, T.R. Jow, J. Power Sources 147 (2005) 234.
[125] G. Liang, L. Wang, X. Ou, X. Zhao, S. Xu, J. Power Sources 184 (2008) 538.
[126] J.K. Kim, G. Cheruvally, J.H. Ahn, H.J. Ahn, J. Phys. Chem. Solids 69 (2008) 1257.
[127] C. Lai, Q. Xu, H. Ge, G. Zhou, J. Xie, Solid State Ionics 179 (2008) 1736.
[128] H.C. Shin, W.I. Cho, H. Jang, Electrochem. Acta 52 (2006) 1472.
[129] K. Kim, J.H. Jeong, I.J. Kim, H.S. Kim, J. Power Sources 167 (2007) 524.
[130] Z.Y. Chen, H.L. Zhu, S. Ji, R. Fakir, V. Linkov, Solid State Ionics 179 (2008) 1810.
[131] V. Palomares, A. Goni, I.G. de Muro, I. de Meatza, M. Bengoechea, I. Cantero, T. Rojo, J. Power Sources 195 (2010) 7661.
[132] A. Fedorkova, A. Nacher-Alejos, P. Gomez-Romero, R. Orinakova, D. Kaniansky, Electrochim. Acta 55 (2010) 943.
[133] S.J. Kwon, C.W. Kim, W.T. Jeong, K.S. Lee, J. Power Sources 137 (2004) 93.

[134] J.K. Kim, G. Cheruvally, J.W. Choi, J.U. Kim, J.H. Ahn, G.B. Cho, K.W. Kim, H.J. Ahn, J. Power Sources 166 (2007) 211.
[135] M. Konarova, I. Taniguchi, J. Power Sources 194 (2009) 1029.
[136] S. Franger, F. Le Cras, C. Bourbon, H. Rouault, J. Power Sources 119 (2003) 252.
[137] H.C. Kang, D.K. Jun, B. Jin, E.M. Jin, K.H. Park, H.B. Gu, K.W. Kim, J. Power Sources 179 (2008) 340.
[138] C.H. Mi, X.G. Zhang, X.B. Zhao, H.L. Li, J. Alloys Compd. 424 (2006) 327.
[139] M. Higuchi, K. Katayama, Y. Azuma, M. Yukawa, M. Suhara, J. Power Sources 119 (2003) 258.
[140] A.V. Murugan, T. Muraliganth, A. Manthiram, Electrochem. Commun. 10 (2008) 903.
[141] S. Beninati, L. Damen, M. Mastragostino, J. Power Sources 180 (2008) 875.
[142] J. Barker, M.Y. Saidi, J.L. Swoyer, Electrochem. Solid State Lett. 6 (2003) A53.
[143] C.W. Kim, M.H. Lee, W.T. Jeong, K.S. Lee, J. Power Sources 146 (2005) 534.
[144] L Wang, G.C. Liang, X.Q. Ou, X.K. Zhi, J.P. Zhang, J.Y. Cui, J. Power Sources 189 (2009) 423.
[145] H.P. Liu, Z.X. Wang, X.H. Li, H.J. Guo, W.J. Peng, Y.H. Zhang, Q.Y. Hu, J. Power Sources 184 (2008) 469.
[146] S. Yang, P.Y. Zavalij, M.S. Whittingham, Electrochem. Commun. 3 (2001) 505.
[147] J. Chen, M.J. Vacchio, S. Wang, N. Chernova, P.Y. Zavalij, M.S. Whittingham, Solid State ionics 178 (2008) 1676.
[148] S. Tajimi, Y. Ikeda, K. Uematsu, K. Teda, M. Sato, Solid State Ionics 175 (2004) 287.
[149] G. Meligrana, C. Gerbaldi, A. Tuel, S. Bodoardo, N. Penazzi, J. Power Sources 160 (2006) 516.
[150] K. Dokko, S. Koizumi, K. Sharaishi, K. Kanamura, J. Power Sources 165 (2007) 656.
[151] M.R. Yang, W.H. Ke, S.H. Wu, J. Power Sources 146 (2005) 539.
[152] J.K. Kim, J.W. Choi, G.S. Chauhan, J.H. Ahn, G.C. Hwang, G.B. Choi, H.J. Ahn, Electrochem. Acta 53 (2008) 8258.
[153] R. Dominko, M. Bele, M. Gaberscek, M. Remskar, D. Hanzel, J.M. Goupil, S. Pejovnik, J. Jamnik, J. Power Sources 153 (2006) 274.
[154] H. Liu, J. Xie, K. Wang, J. Alloys Compd. 459 (2008) 521.
[155] D. Choi, P. Kumta, J. Power Sources 163 (2007) 1064.
[156] F. Gao, Z. Tang, J. Xue, Electrochem. Acta 53 (2007) 1939.
[157] S.L. Bewlay, K. Konstantinov, G.X. Wang, S.X. Dou, H.K. Liu, Mater. Lett. 58 (2004) 1788.
[158] L.N. Wang, Z.G. Zhang, K.L. Zhang, J. Power Sources 167 (2007) 200.
[159] L.N. Wang, X.C. Zhan, Z.G. Zhang, K.L. Zhang, J. Alloys Compd. 456 (2008) 461.
[160] H. Liu, D. Tang, Solid State Ionics 179 (2008) 1897.
[161] M. Maccario, L. Croguennec, A. Wattiaux, E. Suard, F. Le Cra, C. Delmas, Solid State Ionics 179 (2008) 2020.
[162] M. Maccario, L. Croguennec, F. Weill, F. Le Cra, C. Delmas, Solid State Ionics 179 (2008) 2383.